SIMULATION OF SEMICONDUCTOR DEVICES AND PROCESSES Vol. 4
Edited by W. Fichtner, D. Aemmer - Zurich (Switzerland) September 12-14, 1991 - Hartung-Gorre

2D Modelling of Distributed Feedback Semiconductor Lasers

H.-J. Wünsche, H. Wenzel, U. Bandelow, and J. Piprek
FB Physik der Humboldt-Universität zu Berlin, Invalidenstr. 110, D-O-1040 Berlin

H. Gajewski and J. Rehberg
Karl-Weierstraß-Institut für Mathematik, Hausvogteiplatz 10, D-O-1080 Berlin

Abstract

The electronic van Roosbroeck equations are combined with optical wave and coupled mode equations, allowing for wavelength dependent index and gain. Gain dispersion and spectral selectivity is shown to influence drastically the impacts of spatial hole burning in DFB lasers.

Distributed feedback (DFB) lasers exhibit spectral properties, which are very usefull for applications in optical communication systems. A periodic longitudinal corrugation of the internal waveguide (as sketched in Fig.1) is the characteristic feature of these devices. It causes an optical feedback, which strongly depends on the light frequency ω. Therefore, a correct modelling of such lasers should consider the spectral dependencies of the gain and other optical quantities. All 2D simulations of laser diodes reported until now (e.g., [1]) consider Fabry-Perot (FP) configurations only.

In our paper, we shall describe a first 2D model for DFB lasers. Electrically, the transverse plane of the laser diode is described by the well known van Roosbroeck semiconductor device equations, which are solved numerically by our finite element simulation code TOSCA, extended to the case of heterodevices (cf. Fig.2). Since laser action principially requires degenaracy of carriers, Fermi statistics is adopted.

The optical part of the model consists of two equations for the main component of the electric field (Λ is the corrugation period)

$$\mathcal{E}(\vec{r},t) = [a(z)e^{-i\frac{\pi}{\Lambda}z} + b(z)e^{i\frac{\pi}{\Lambda}z}]\; E(x,y)\; e^{i\omega t}. \tag{1}$$

First, the transverse field shape is determined by the wave equation

$$[\; \frac{\partial^2}{\partial x^2} + \frac{\partial^2}{\partial y^2} + (\frac{\omega}{c}\bar{n}(\omega) + \frac{i}{2}g(\omega))^2 \;]\; E_\nu(x,y) = \beta_\nu(\omega)^2 E_\nu(x,y), \tag{2}$$

where ν numbers the different transverse modes. The dependences of the refractive index $\bar{n}(\omega)$ and the material gain $g(\omega)$ on the carrier densities n and p are modeled by

$$\bar{n}(\omega) = \bar{n}_0(\omega) + \bar{n}' \cdot (n + p - |N_D - N_A|), \tag{3}$$

$$g(\omega) = g_0 \cdot \sqrt{\frac{\hbar\omega - E_g}{kT}} \cdot f_n \cdot f_p \cdot \{1 \; - \; \exp\frac{\hbar\omega + F_p - F_n}{kT}\}, \tag{4}$$

with f_n, f_p being the occupation numbers of electrons and holes, respectively, and F_n, F_p the corresponding quasi Fermi levels. In our examples, we use $\bar{n}' = -10^{-20} cm^3$, $g_0 = 2250 cm^{-1}$ and

the formulae of Burkhardt [2] for the intrinsic refractive index $\bar{n}_0(\omega)$. The material gain $g(\omega)$ is depicted in fig.3. It is treated perturbationally when solving the wave equation. Mathematically, (2) is an eigenvalue problem for an elliptic equation over a finite domain. The discretization is carried out by the same finite element approach as for the van Roosbroeck system, but different boundary conditions have to be imposed. The discretized eigenvalue problem is solved by inverse vector iteration. Fig.4 illustrates the dispersion of the two lowest ($\nu = 0$ and 1) Eigenvalues $\beta_\nu(\omega)$.

Second, the amplitudes $a(z)$ and $b(z)$ of the forward and backward travelling waves in (1) obey the so called coupled mode equations [3]

$$i\frac{\partial a}{\partial z} = (\beta_m - \frac{\pi}{\Lambda})a + \kappa^+ b \qquad \text{and} \qquad -i\frac{\partial b}{\partial z} = (\beta_m - \frac{\pi}{\Lambda})b + \kappa^- a. \tag{5}$$

The coupling coefficients $\kappa^\pm$ depend on the concrete kind of corrugation and on the transverse field shape. For demonstration purposes, we shall treat them as independent parameters. Completed by reflecting boundary conditions at the laser facets, these equations define another set of complex Eigenvalues β_m, called longitudinal modes. The dependence on $\kappa^\pm$ of the seven modes closest to the Bragg value π/Λ are shown in Fig.5 for the case of index-coupling. The real parts shift away from the Bragg value with increasing κ. The imaginary parts, which represent the longitudinal losses, decrease and depend considerably on the mode number m. In the limit $\kappa \to 0$, they approach to the Fabry-Perot value, which is independent of m.

The individual equations (2) and (5) are coupled with each other by physical conditions. Equating the real parts of both β yields the frequencies $\omega_{\nu m}$ of the complete laser modes. The modal gain represented by $Im[\beta_\nu(\omega_{\nu m})]$ *must not* be larger than the modal losses $Im[\beta_m]$ for any mode νm. Furthermore, only those modes with equal gains and losses (threshold condition) can carry optical power $P(\omega_{\nu m}) > 0$. They feed back to the electrical equations via their contribution

$$R_{stim}(\omega_{\nu m}) = \bar{n}(\omega_{\nu m})\; g(\omega_{\nu m})\; P(\omega_{\nu m})\; |E_\nu(x, y, \omega_{\nu m})|^2, \tag{6}$$

to the stimulated recombination (appropriate normalization of E_ν supposed).

We use an effective three step method for solving the coupled set of equations. In a first step, the coupled van Roosbroeck and wave equations are solved selfconsistently in the x, y-plane with treating not only the bias U, but also the frequency ω and the optical Power P of the fundamental mode $\nu = 0$ as independent *external parameters* (the power in the mode $\nu = 1$ is assumed to vanish). Result is a table containing the values of β_ν as functions of U, P and ω. Secondly, another table with the β_m is obtained by solving the coupled mode equations (5). Combining both types of tables in the third step, we get all modal frequencies $\omega_{\nu m}$, the number l of the lasing longitudinal mode and the power $P(\omega_{0l})$ carried by it from the equations

$$Re[\beta_\nu(\omega_{\nu m}) - \beta_m] = 0 \qquad \text{and} \qquad \max_m\; Im[\beta_0(\omega_{0m}) - \beta_m] = 0, \tag{7}$$

where l realizes the maximum and P makes it zero.

Using this model, we compare the roles of spatial hole burning in FP and DFB lasers. Hole burning in the lateral carrier distribution (Fig.7) decreases the gain of the $\nu = 0$ mode relative to that with $\nu = 1$ (Fig.4c).

In a usual FP laser, where the losses $Im(\beta_m)$ are independent of m, the maximum of the gain curve $Im[\beta_0(\omega)]$ is clamped at this value above threshold, as illustrated in Fig.6a. As can be seen, the corresponding gain curves of the $\nu = 1$ mode (dashed), are not clamped as well

Figure captions

Fig.1 Schematic view of the buried ridge DFB laser, which is considered in the numerical examples. Lateral symmetry allows to confine the simulation to one half of the device. Typical values for $\lambda = 1.55\mu m$ have been assumed for the model parameters, which cannot be presented for briefity.

Fig.2 The 2D shape of the conduction band edge in the high injection regime.

Fig.3 Dependence of the gain in the active material on the wavelength $\lambda = 2\pi c/\omega$ for different excess carrier densities. It vanishes for wavelengths above the gap-wavelength ($\lambda_g = 1.55\mu m$) and changes its sign at a "Fermi-wavelength", which corresponds to the difference $F_n - F_p$ of the quasi Fermi levels.

Fig.4 Dispersion of the transverse mode eigenvalues β_ν. U denotes the bias applied to the laser diode. The real part (a) depends only weekly on bias U and power P. The imaginary part (b) (gain of the mode) recovers qualitatively the shape of the material gain. The $\nu = 1$ gain is smaller then that for $\nu = 0$, due to smaller optical confinement. Optical power reduces the modal gains drastically (c) due to decreasing the carrier densities by stimulated recombination. Spatial hole burning (cf. Fig.7) decreases the $\nu = 0$ gain below that for $\nu = 1$.

Fig.5 Dependence of some lowest eigenvalues β_m of the coupled mode equations on the coupling constant κ ($= \kappa^+ = \kappa^-$, index coupling). R denotes the power reflectivities at both laser facets and L the laser length.

Fig.6 Illustration of the different threshold and hole burning behaviours of FP (a) and DFB (b) lasers. (Length $L = 200\mu m$ and width $W = 2\mu m$ of the active zone in both cases.) Both the longitudinal and transverse modes are drawn in the complex β-plane. The longitudinal modes β_m are discrete values (crosses), the transverse β_ν are contineous curves for every ν (cf. Fig.4). The real parts of β_m lie very close (only every second one has been drawn in (a)!). The vertical distance from a cross to a transverse curve is the net gain, i.e., the difference between the gain of the transverse modes and the longitudinal losses. It is negative for all m at low bias and $P = 0$ (below threshold). The threshold is reached, when the maximum net gain approaches zero with still $P = 0$. With a FP laser this occurs (approximately) at the maximum of the transverse gain, with a DFB laser at the minimum of $Im(\beta_m)$. With further increasing bias (above threshold), the net gain at these positions must not further increase, which is ensured by a finite optical power P in mode $\nu = 0$. The further slight increase of the net gain of mode $\nu = 1$ is due to the spatial hole burning.

Fig.7 Lateral distribution of the optical intensities and the material gain in the active zone at a power of $100mW$ in mode $\nu = 0$ at $\lambda = 1.50\mu m$. The gain shows a clear hole at the center of the active region, it is larger at the position of the mode $\nu = 1$.

Fig.8 Critical powers P_c for the laser onset of the mode $\nu = 1$ in dependence on the width W of the active zone for a FP-laser and three DFB-lasers. The labels at the curves indicate the Bragg period Λ in nm.

but continue rising. This is due to the transversal hole burning. At a critical power P_c, they reach the losses and start to lase, too. Above this point, they should be also clamped. This is not reflected in Fig.6, due to our assumption of vanishing power in the mode $\nu = 1$, which is not valid above P_c. Nevertheless, P_c can be correctly estimated from below. It's dependence on the width W of the active zone is drawn in Fig. 8.

In a DFB laser, the losses $Im(\beta_m)$ have a deep and sharp minimum at $Re(\beta_m) \approx \pi/\Lambda$ (Fig.6b) and the gain of the lasing mode $\nu = 0$ is clamped at this position. Since the neighbouring $Im(\beta_m)$ are much larger, the mode $\nu = 1$ may remain unlasing, although spatial hole burning increases its maximum gain above that of the fundamental mode. Therefore, the critical power P_c now depends not only on W, but also on Λ and κ. Few examples are presented in Fig.8. A systematic study will be published later.

References

[1] G. H. Song, K. Hess, T. Kerkhoven, and U. Ravaioli: "Twodimensional simulator for semiconductor lasers", Proc. of the Intern. IEEE Electron Device Meeting, Washington 1989, p. 143.

[2] H. Burkhardt: "Effective phase and group indices for $In_{1-x}Ga_xP_{1-y}As_y/InP$ waveguide structures", J. Appl. Phys. 55 (1984), p. 503.

[3] G. P. Agrawal and N. K. Dutta: "Long-Wavelength Semiconductor Lasers", van Nostrand Reinhold, New-York 1986, chapter 7.

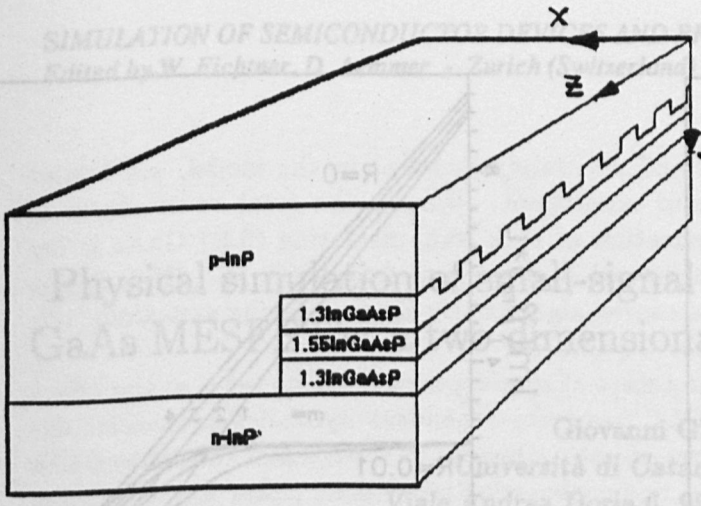

Fig. 1

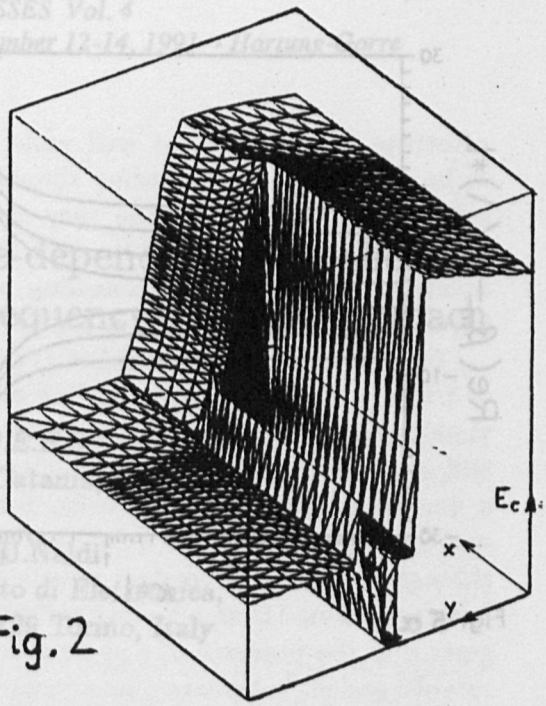

Fig. 2

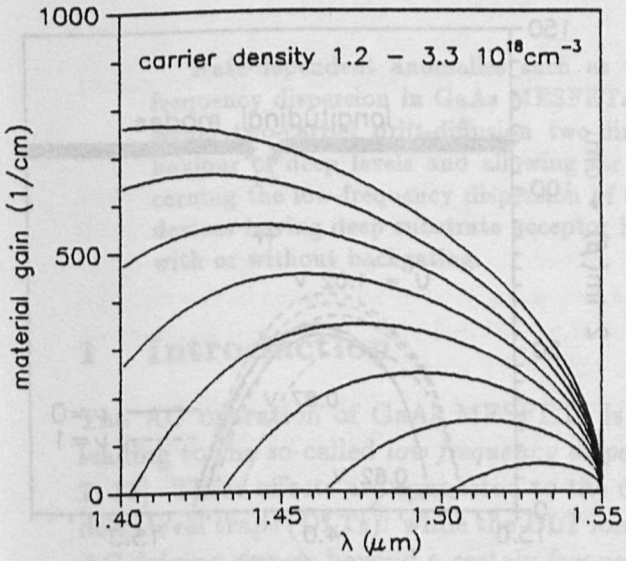

Fig. 3

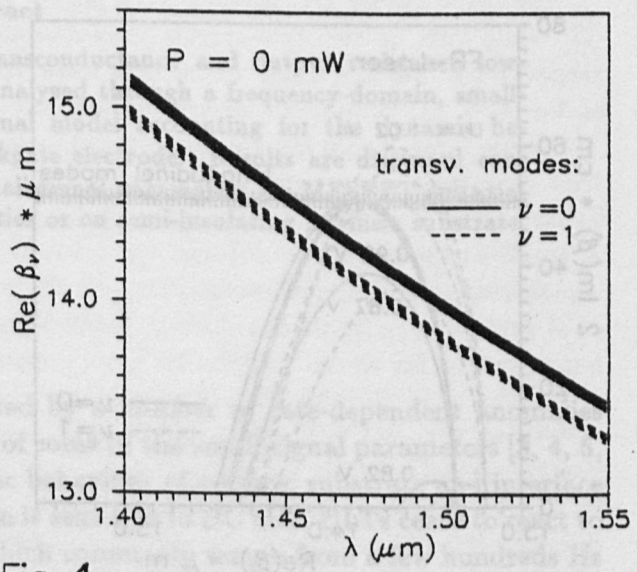

Fig. 4a

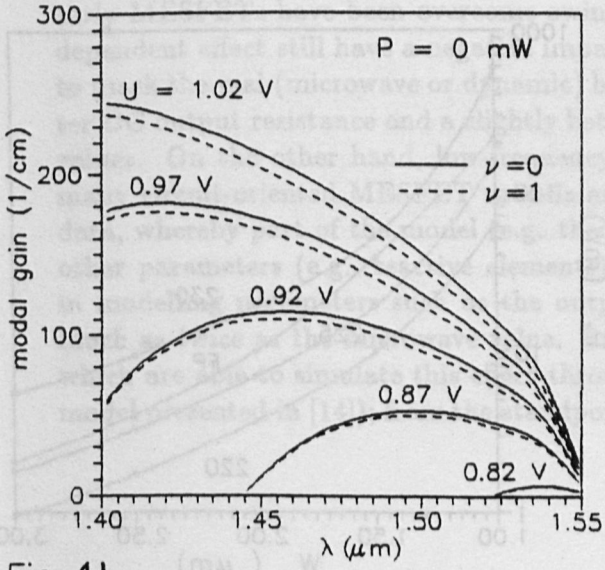

Fig. 4b

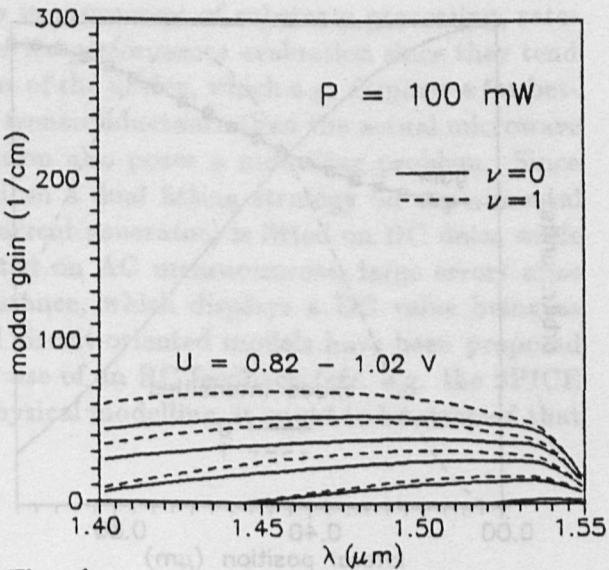

Fig. 4c

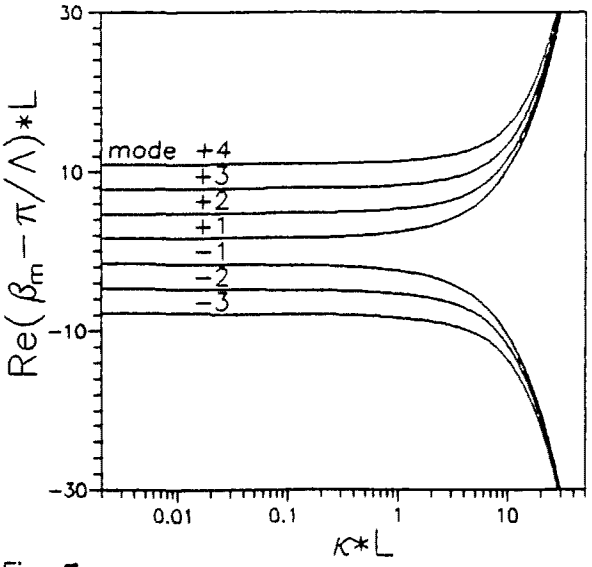

Fig. 5a

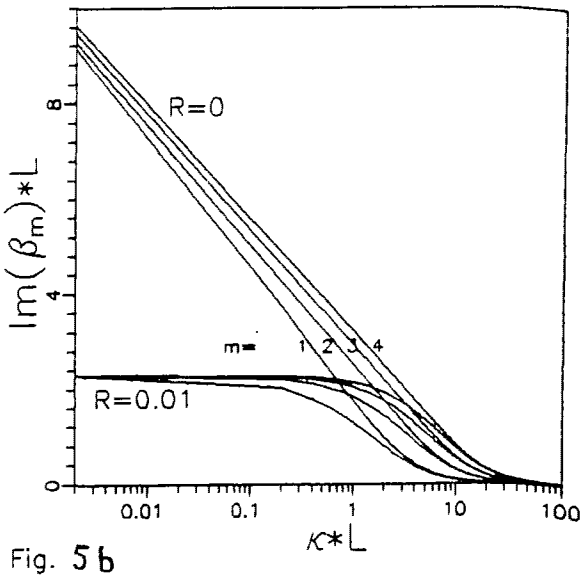

Fig. 5b

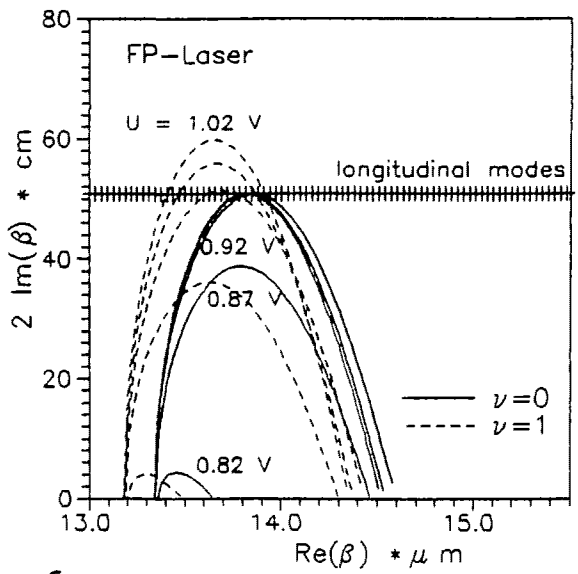

Fig. 6a

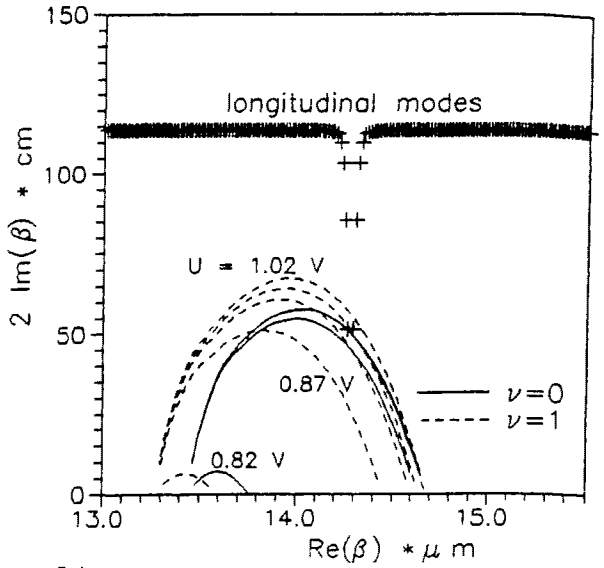

Fig. 6b

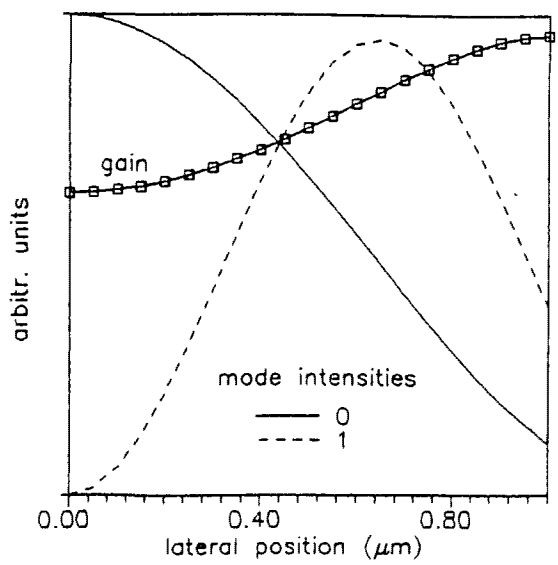

Fig. 7

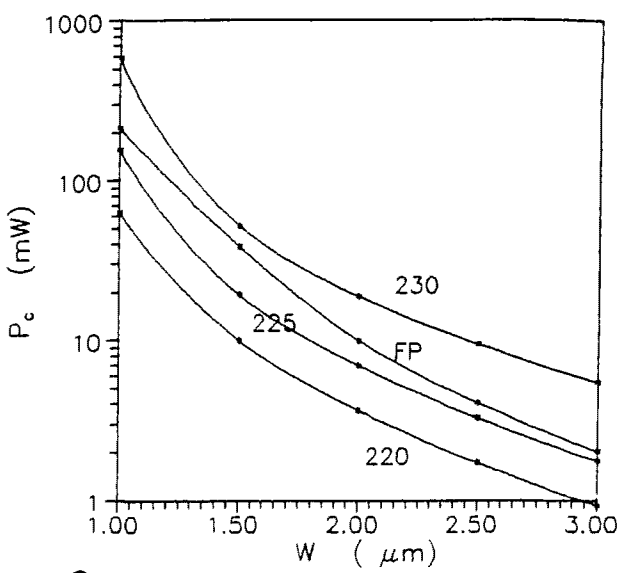

Fig. 8